



Preparation of BiPO₄ nanosphere and its enhanced photocatalytic activity under simulated solar light degradation of tetracycline

Zhongjie Zhang^a, Xiaojun Huang^a, Jingru Guo^a, Yajie Du^a, Liping Wang^a, Changyu Lu^{b,c,*}

^aKey Laboratory of Subsurface Hydrology and Ecological Effects in Arid Region, Ministry of Education, School of Water and Environment, Chang'an University, Xi'an 710064, Shaanxi, China, emails: fjish@163.com (Z. Zhang), 532644738@qq.com (X. Huang), GuoJR329602@gmail.com (J. Guo), 1076098267@qq.com (Y. Du), lipingwang1528@chd.edu.cn (L. Wang)

^bSchool of Water Resources and Environment, Hebei Province Key Laboratory of Sustained Utilization and Development of Water Resources, Hebei Province Collaborative Innovation Center for Sustainable Utilization of Water Resources and Optimization of Industrial Structure, Hebei GEO University, Shijiazhuang 050031, China, Tel. +86-29-82334561; Fax: +86-29-82334566; email: pzpzlxl@163.com (C. Lu)

^cSchool of Geology and Environment, Xi'an University of Science and Technology, Xi'an 710064, Shaanxi, China

Received 10 October 2019; Accepted 25 February 2020

ABSTRACT

As an effective and eco-friendly method, photocatalysis is a promising candidate for degrading tetracycline in aqueous solutions. In this work, a highly efficient BiPO₄ nanosphere photocatalyst was successfully synthesized via a simple and facile hydrothermal method. The morphology, structure, optical properties, elemental composition, surface area and photoluminescence of the BiPO₄ nanospheres were characterized by scanning electron microscopy, X-ray diffraction, UV-Vis, X-ray photoelectron spectroscopy and Brunauer–Emmett–Teller adsorption. Compared with the irregular BiPO₄ particles, the BiPO₄ nanospheres exhibited excellent photocatalytic activity for tetracycline (40 mg/L) degradation under simulated solar light irradiation. The rate constant was 0.00783 min⁻¹, which is up to 1.8 times as high as that of pure irregular BiPO₄ particles. The improvement is ascribed to their unique morphology and smaller particle size. According to the electron spin resonance spectroscopy experiments, [•]OH and [•]O₂ were testified to be the predominant active species. This work is expected to provide a possible design of BiPO₄ nanosphere photocatalysts for the mitigation of environmental problems.

Keywords: BiPO₄ nanosphere; Photocatalysis; Tetracycline

1. Introduction

With the rapid development of the pharmaceutical industry, especially the appearance of antibiotics, water pollution has become very rigorous. Antibiotic wastewater is a high concentration of organic wastewater containing materials that are difficult to degrade as well as toxic biological substances [1–3]. Tetracycline (TC) is a kind of antibiotic that is widely used in various fields [4]. However, because

of the unreasonable disposition and their un-metabolized forms through urine and feces of users, antibiotics, which are listed as a kind of “merging organic contaminants”, have been detected in surface water and groundwater, which causes the potential pressure on the ecosystem balance and poses a great threat to human health [5,6]. Therefore, the removal of TC from wastewater is an urgent problem. Furthermore, many methods are used for the governance of antibiotic wastewater. Conventional methods, such

* Corresponding author.

as chemical and biological methods, are limited by their potential risk of secondary contamination and by their low efficiency and high cost [7,8]. It is imperative to find a reasonable and effective method to treat antibiotic wastewater.

Photocatalysis is an advanced oxidation process [9,10], which has received much attention in recent years due to its utilization of renewable and clean energy resources [11–13]. In 1972, Fujishima and Honda were the first to discover the photolysis of water on a TiO_2 electrode [14]. Since then, photocatalytic technology has received widespread attention. In the past 40 y, numerous semiconductor materials (e.g. TiO_2 [15], ZnO [16], C_3N_4 [17], CoO [18], WO_3 [19], etc.) have been studied, which can be used to degrade toxic and harmful substances in water but also has some shortcomings. Nevertheless, most of the above photocatalysts still suffer from kinds of limits, for example, the rapid recombination of electron-hole pairs, instability, and width of band gaps, etc., [20]. Consequently, the search for a more efficient new catalyst is extremely desirable.

As new photocatalysts, bismuth-based semiconductor materials and their inorganic compounds attract much attention due to their substantial photocatalytic activity, stable chemical properties and strong absorption of visible light [21]. In recent years, bismuth phosphate (BiPO_4) has drawn increasing attention among Nobel-metal-free photocatalysts since the firstly reported its photocatalytic activity on degradation of dye by Zhu's Group in 2010 [22]. It is well known that BiPO_4 shows three different modifications, including the monoclinic phase, monazite-type structure and hexagonal phase, with the monazite-type structure the most favored thermodynamically [23]. On the one hand, PO_4^{3-} has a big negative charge to make the dipole distance of bismuth phosphate photocatalyst, which greatly increased and enables us to separate holes and photo-induced electron efficiently [24]. On the other hand, the higher density of electron cloud on the PO_4^{3-} makes the catalyst more inclined to repel electrons and attract holes to inhibit the recombination of holes and electrons. Hence, BiPO_4 has profound application potential in photocatalytic oxidation due to its stable structure, strong UV response, special optoelectronic properties, low cost, etc. However, similar to TiO_2 , the wide band-gap ($E_g \approx 3.85$ eV) lead to weak response to visible light and low utilization of light energy, which results in its low catalytic activity and severely limits the further application of BiPO_4 [25]. The photocatalytic performance of BiPO_4 is confined by the poor quantum yield resulting from the low separation rate of photogenerated electron-hole pairs. Over the years, various efforts have been made to enhance the photocatalytic activity of BiPO_4 , such as surface precious-metal deposition [26], element-doping [27], forming heterojunction [28], and so on. Furthermore, the particle size control and morphology control also plays a very big role before the above modification, which optimized surface performance and improves the band gap. When the conduction band potential of BiPO_4 is more negative than the potential of $\text{O}_2/\cdot\text{O}_2^-$ (-0.33 eV vs. NHE), which implies that O_2 can be reduced to generate $\cdot\text{O}_2^-$ and improve the photocatalytic degradation performance.

In this work, a simple hydrothermal method was used to synthesize BiPO_4 nanospheres to achieve the purpose of morphology control. In comparison with irregular BiPO_4

particles, as-prepared BiPO_4 nanospheres show superior photocatalytic activity. Moreover, a series of characterization experiments were carried out using BiPO_4 nanospheres and irregular BiPO_4 particles to investigate the photocatalytic activity.

2. Material and methods

2.1. Material

All chemicals in this study were of analytical grade without any further purification. Disodium hydrogen phosphate dihydrate ($\text{Na}_2\text{HPO}_4 \cdot 12\text{H}_2\text{O}$) and phosphoric acid (PVP) were obtained from Tianjin Kemiou Chemical Reagent Co., Ltd., China. Ethanol and phosphoric acid were obtained from Tianjin Tianli Chemical Reagent Co., Ltd., China.

2.2. Preparation of catalysts

In a typical synthesis process, 3 mmol $\text{Bi}(\text{NO}_3)_3 \cdot 5\text{H}_2\text{O}$ was dissolved into 100 ml of ethylene glycol. Then, 3 mmol $\text{Na}_2\text{HPO}_4 \cdot 12\text{H}_2\text{O}$ was added into the solution, and the solution was stirred for 15 h at room temperature. The precipitates were washed with ethanol three times at 11,000 *r* speed. Next, 60 ml 2 mol/L phosphoric acid aqueous was added to the precipitates. Subsequently, the mixed solution was transferred to a 100 ml Teflon-lined stainless steel autoclave and was then heated to 160°C for 6 h. The precipitate was collected by centrifugation, washed with ethanol three times, and dried at 60°C for 24 h before being ground into powder. Finally, the BiPO_4 nanospheres were obtained.

The preparation method used for the irregular BiPO_4 particles is similar to the above method. The differences are the use of ultrasonic treatment for 30 min instead of stirring before the transfer of the above-mixed solution to a 100 ml Teflon-lined stainless steel autoclave, followed by heating to 190°C for 24 h.

2.3. Characterization

The products were systematically characterized using different techniques. The X-ray diffraction (XRD) patterns were determined at room temperature with a Bruker, Germany D8 Advanced X-ray powder diffractometer with $\text{Cu K}\alpha$ radiation ($k = 1.5406$ Å). The testing voltage was 40 KV and the scanning range was 10°–90°. The size and morphology of the BiPO_4 nanospheres were obtained via scanning electron microscopy (SEM) with a Hitachi S-4800 electron microscope (The Japanese). UV-Vis absorption spectra were measured by a Shimadzu Model 2550 (Japan) with an integrating sphere in the wavelength range of 200–900 nm by using barium sulfate for reference. X-ray photoelectron spectroscopy (XPS) valence band spectra of the sample were determined by a K-alpha XPS system (Thermo Fisher, USA) with K-alpha irradiation as the excitation source and the C 1s binding energy of 284.6 eV as the internal standard. A Tristar II Plus 2.02 automatic surface area and pore analyzer was used to evaluate the Brunauer–Emmett–Teller (BET) surface areas (A_{BET}) and porosity of the as-prepared samples. The electron spin resonance (ESR) spectroscopy signals were measured using a Bruker ER200-SRC spectrometer to

further detect the presence of $\cdot\text{OH}$ and $\cdot\text{O}_2^-$ radicals in the photocatalytic reaction system under 300 W xenon lamp irradiation.

2.4. Evaluation of photocatalytic activity

For photocatalytic experiments, 15 mg photocatalyst was suspended in 50 ml aqueous solution of 40 mg/L TC. The lamp-to-sample distance is 8 cm and the pH of the TC solutions is 6.8. The aqueous solution was stirring for 30 min in the dark to reach adsorption equilibrium. Then, the aqueous solution was exposed to light (300 W, xenon lamp) irradiation under magnetic stirring. At certain time intervals, a 4 ml aqueous solution was sampled and centrifuged to remove the photocatalyst particles. Then, the aqueous solution was analyzed by an ultraviolet spectrophotometer to obtain the concentration of TC. Finally, the degradation rate was calculated by the following Eq. (1):

$$\text{Degradation}(\%) = \left(1 - \frac{A_i}{A_0}\right) \times 100\% \quad (1)$$

where A_0 is the absorbance of the initial solution and A_i is the absorbance of the solution after the reaction.

3. Results and discussion

3.1. X-ray diffraction

The phase identity and crystal structures of the BiPO_4 nanospheres and irregular BiPO_4 particles were determined by XRD and are shown in Fig. 1. The XRD patterns of the as-formed BiPO_4 nanospheres contained strong peaks at $2\theta = 21.4^\circ, 27.2^\circ, 29.1^\circ, 31.2^\circ, 34.5^\circ, 36.1^\circ,$ and 42.9° , corresponding to the $(-111), (120), (210), (012), (-202), (020),$ and (-103) crystalline phases of the monoclinic BiPO_4 structure (JCPDS No. 15-0767) [29]. No impurity peaks appeared in the XRD patterns, indicating the high purity of the products. Compared with the BiPO_4 nanospheres, the irregular BiPO_4 particles had sharper diffraction peaks, indicating that the as-formed product had a relatively high crystallinity. Simultaneously, the most intense peak (120) indicated the growth direction of the morphology for the two different samples.

3.2. Scanning electron microscopy

The morphology and structure of the as-prepared BiPO_4 characterized using SEM. Fig. 2a shows the high and low magnified SEM images of the BiPO_4 nanospheres. The diameter of the microspheres ranged from 80–150 nm. Nanostructures are ideal candidates for the study of the dependence of the structural and optical properties on the quantum confinement effect. According to the surface effect, the smaller particle size can provide more surface atoms and larger area so that the catalyst has a higher catalytic activity. Fig. 2b shows the SEM images of the irregular BiPO_4 particles. The particles were observed to be wildly disordered and agglomerated, with irregular morphology. In addition, the diameter of the particles was larger than that of the nanospheres. Hence, it can be concluded that the

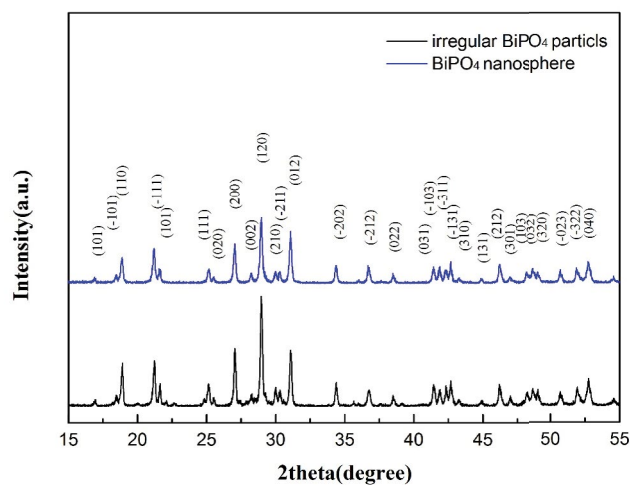


Fig. 1. XRD patterns of BiPO_4 nanospheres and irregular BiPO_4 particles.

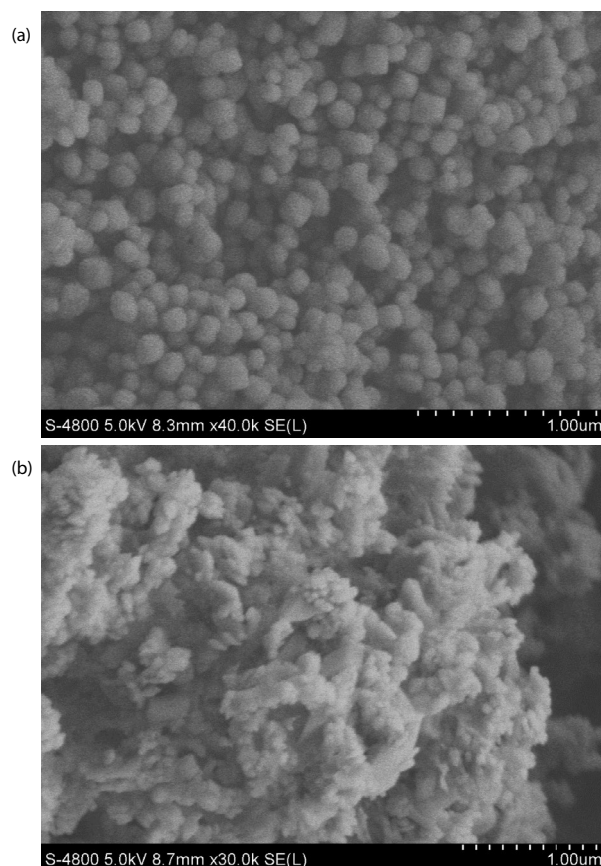


Fig. 2. SEM images of (a) BiPO_4 nanospheres and (b) irregular BiPO_4 particles.

nanospheres should show better photocatalytic properties compared to the irregular particles.

3.3. UV-vis spectroscopy

The optical properties of the BiPO_4 nanospheres and the irregular BiPO_4 particles were characterized by UV-Vis

absorption spectra, and the results are shown in Fig. 3. The light absorption edges of the BiPO₄ nanospheres and the irregular BiPO₄ particles appear at about 400 and 300 nm, respectively. As shown in Fig. 3a, when the wavelength is larger than 260 nm, the intensity of the absorption of light energy for the BiPO₄ nanospheres is slightly higher than the irregular BiPO₄ nanoparticles. It can be concluded that the nanospheres show a better optical response compared to the irregular BiPO₄ particles. However, the response of the two samples in the visible region is not obvious. This result can be attributed to the wide band gap of BiPO₄. As shown in Fig. 3b, the E_g can be calculated according to Tauc equation [30] as follows:

$$\alpha h\nu = A[h\nu - E_g]^{n/2} \quad (2)$$

where α , h , ν and A is absorption coefficient, Planck constant, light frequency and a constant, respectively. For indirect transition material BiPO₄, the n value equal to 4, respectively [31]. The calculated band gaps of the BiPO₄ nanosphere were 4.48 eV. To get the position of valence bands accurately,

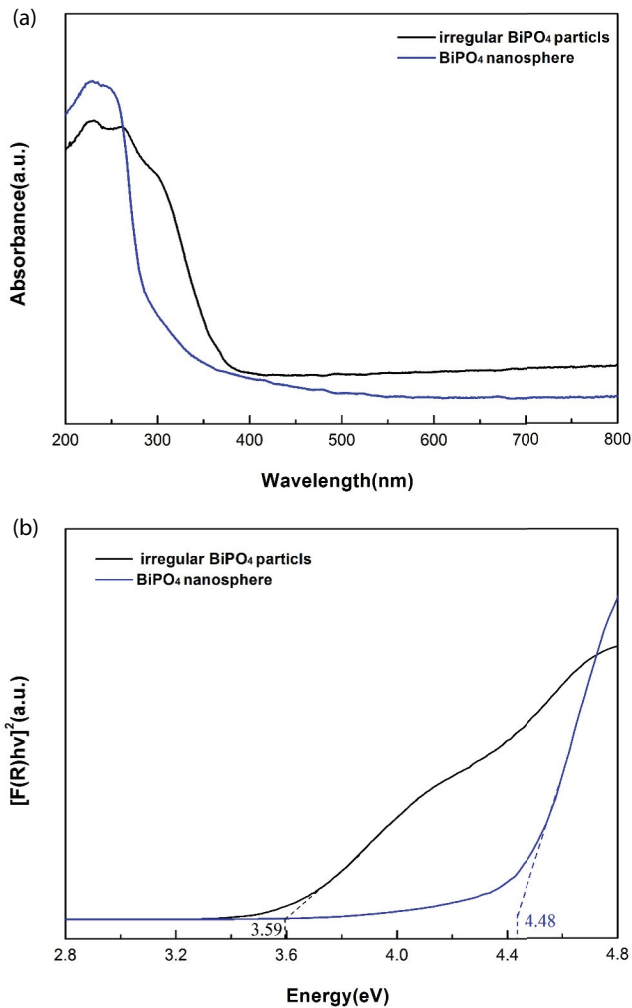


Fig. 3. (a) UV-vis diffuse reflectance spectra and (b) Tauc plot of BiPO₄ nanospheres and irregular BiPO₄ particles.

XPS valence band spectra were employed to analyze the BiPO₄ nanosphere. In Fig. 4, the BiPO₄ nanosphere displayed a typical valence band (VB) density of states with the edge of the maximum energy at about 3.97 eV, and the calculated conduction band (CB) was -0.51 eV.

3.4. XPS analysis and valence band spectra

XPS spectra were used to investigate the surface chemical composition and chemical status of elements of the BiPO₄ nanospheres. The XPS survey spectrum is shown in Fig. 5a demonstrates that Bi, P and O are the main elements. The high-resolution XPS spectrum of Bi 4f is shown in Fig. 5b, which shows two typical peaks at approximately 161.69 and 167.19 eV that are ascribed to the binding energies of Bi 4f_{7/2} and Bi 4f_{5/2} indicating the existence of a trivalent oxidation state for Bi [32]. As shown in Fig. 5c, the binding energy of P 2p was 135.09 eV, indicating an oxidation state of P⁵⁺ in the BiPO₄ [33]. In Fig. 5d the characteristic peak at 533.17 eV can be attributed to the O 1s spectrum, demonstrating the presence of the crystal lattice oxygen (O²⁻) in the BiPO₄.

3.5. Brunauer–Emmett–Teller

Fig. 6 demonstrates the N₂ adsorption and desorption isotherms of the BiPO₄ nanospheres and the irregular BiPO₄ particles. As shown in Fig. 6, both isotherms were of type IV, according to the International Union of Pure and Applied Chemistry classification, with an H3 hysteresis loop observed in the range of $P/P_0 \approx 0.15$ –1.00, confirming the presence of mesopores (2–50 nm) [34]. As expected, the BiPO₄ nanospheres showed a larger specific surface area (8.2870 m²/g) than the irregular BiPO₄ particles (3.3895 m²/g), indicating that the high specific surface area is likely to contribute to the improvement of photocatalytic activity profiting from more surface active sites.

3.6. Photocatalytic performance

The photocatalytic degradation towards TC as a model pollutant in aqueous solution under Xenon lamp irradiation

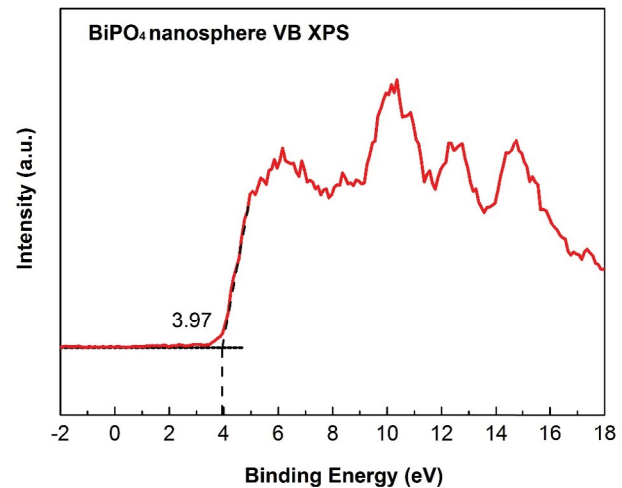


Fig. 4. XPS valence band spectra of BiPO₄ nanospheres.

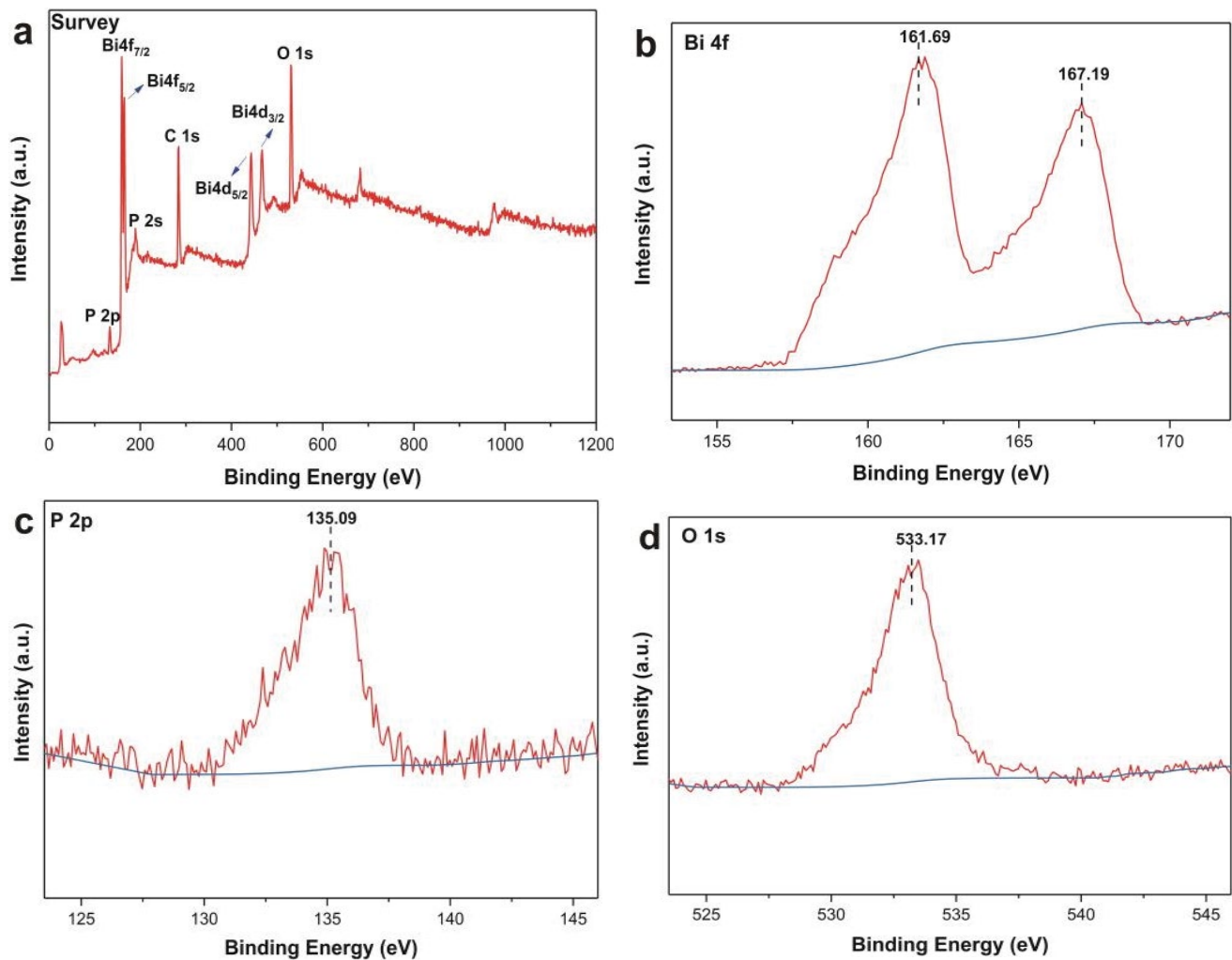


Fig. 5. XPS spectra for the BiPO_4 nanospheres: (a) survey spectrum of the sample, (b) Bi 4f, (c) P 2p, and (d) O 1s.

was performed for the BiPO_4 nanospheres and the irregular BiPO_4 particles. The aqueous TC and photocatalyst were magnetically stirred in the dark for 30 min. At this point, the degradation of TC was mainly due to the adsorption of the catalyst. Fig. 7a shows that the dark adsorption equilibrium is established after 30 min. The adsorption content of BiPO_4 nanospheres is better than that of irregular BiPO_4 particles, which is consistent with the results of BET presented in the previous paragraph. As expected, when light irradiates the photocatalysts, the BiPO_4 nanospheres show an excellent photocatalytic activity compared to the irregular BiPO_4 particles. A possible reason for this enhanced activity is that the special globular morphology and the smaller particle size of the BiPO_4 provides a larger surface as well as more surface reactive sites, as demonstrated by the BET analysis. As shown in Fig. 7c, after 90 min irradiation, the removal rate of the BiPO_4 nanospheres and the irregular BiPO_4 particles reached 47.3% and 31.5%, respectively.

We used the pseudo-first-order model to investigate the kinetic rate constants for the degradation of TC, which can be expressed as:

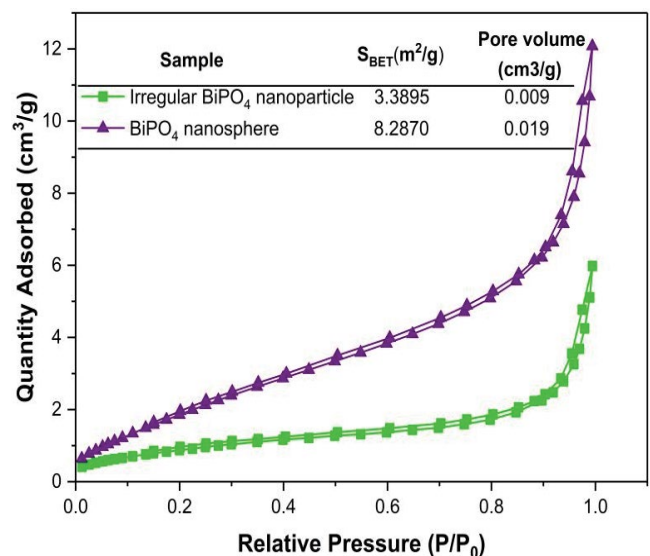


Fig. 6. Nitrogen sorption isotherm and measured parameters (inset).

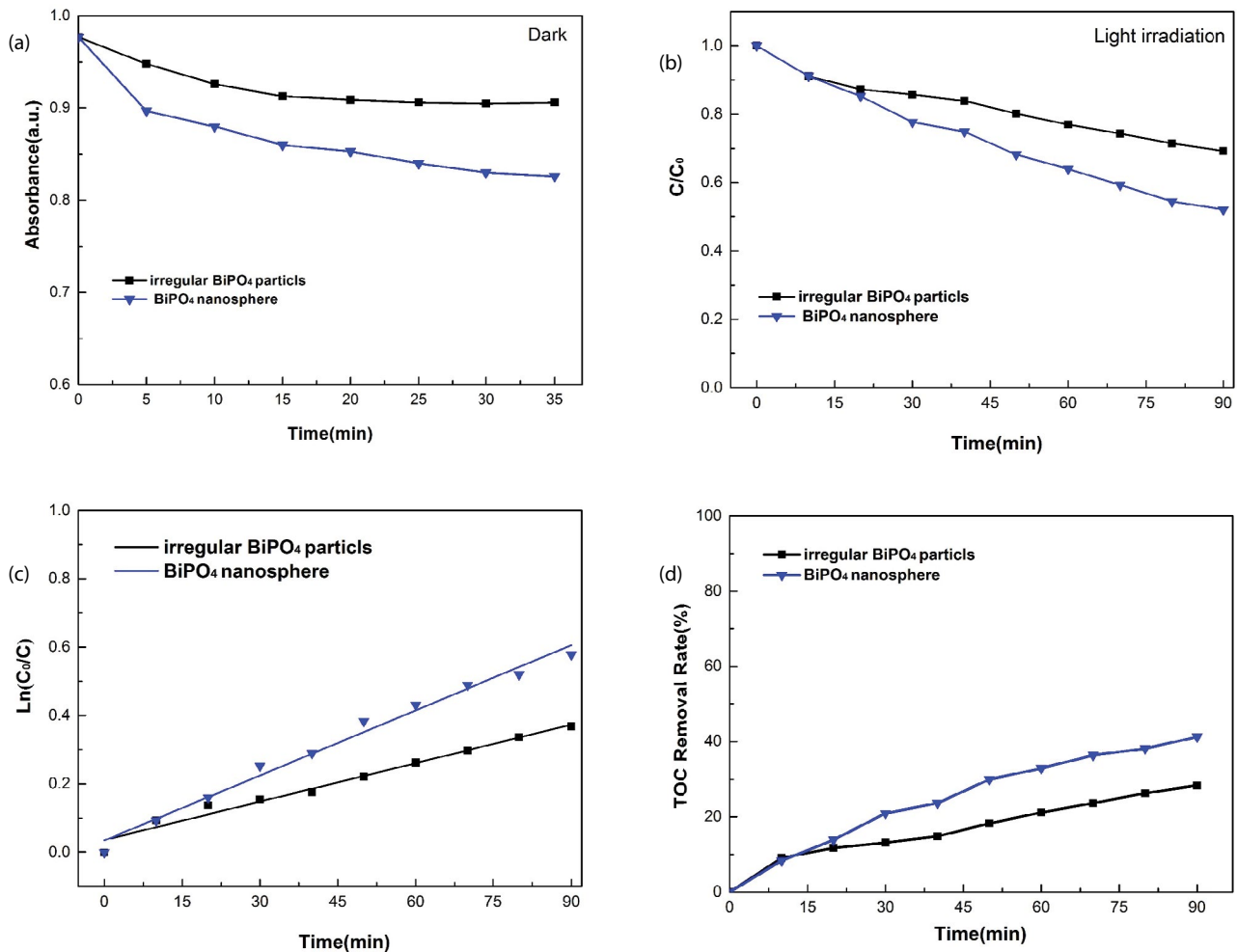


Fig. 7. (a) Absorption properties under dark conditions, (b) photocatalytic degradation, (c) apparent rate constants, and (d) TOC removal of TC on BiPO₄ nanospheres and irregular BiPO₄ particles.

$$\ln\left(\frac{C_0}{C}\right) = K_{app}t \quad (3)$$

where K_{app} is the first-order rate constant, C_0 (mg/L) is the initial concentration of TC, and C (mg/L) is the concentration of TC at an irradiation time t . As shown in Fig. 7c, kinetic rate constants for the degradation of TC by the BiPO₄ nanospheres followed a pseudo-first-order kinetics plot. The value of the reaction rate for the BiPO₄ nanospheres was 0.00783 min⁻¹, which is 1.8 times higher than that for the irregular BiPO₄ particles. Total organic carbon (TOC) analysis is an effective method that can be used to further demonstrate the mineralization of organic pollutants. In Fig. 7d, the removal rates of TOC of BiPO₄ nanospheres and irregular BiPO₄ particles were 41.6% and 28.2%, respectively. TOC contents decreased in the same order as that of the photocatalytic degradation curves. However, the removal rates of TOC were lower than that of the degradation. This result was reasonable due to the degradation data were detected after centrifugation. Moreover, widely environmental applications, such as the mineralization, would be implemented by BiPO₄ since the reduced TOC contents suggested.

3.7. Electron spin resonance spectroscopy

To investigate the photocatalytic mechanism of BiPO₄ nanospheres, a spin-trapping ESR experiment is performed to verify the existence of $\cdot\text{OH}$ and $\cdot\text{O}_2^-$ species. As displayed in Fig. 8, no ESR signals could be found under dark conditions. However, the characteristic signals of DMOP- $\cdot\text{OH}$ and DMPO- $\cdot\text{O}_2^-$ appeared under xenon lamp irradiation, which uncovers that DMOP- $\cdot\text{OH}$ and DMPO- $\cdot\text{O}_2^-$ can be generated and take part in the photocatalytic degradation reaction.

3.8. Photocatalytic degradation mechanism

Based on the above result, a mechanism was proposed based on charge separation and the photocatalytic process of the BiPO₄ nanospheres, as shown in Fig. 9. According to the result of the Tauc equation, the positions of the VB and CB of BiPO₄ nanospheres are 3.97 and -0.51 eV (vs. NHE), respectively. Under solar light irradiation, photo-excited electrons were generated in the VB of the BiPO₄ nanospheres, which then transited into the CB. Because the CB

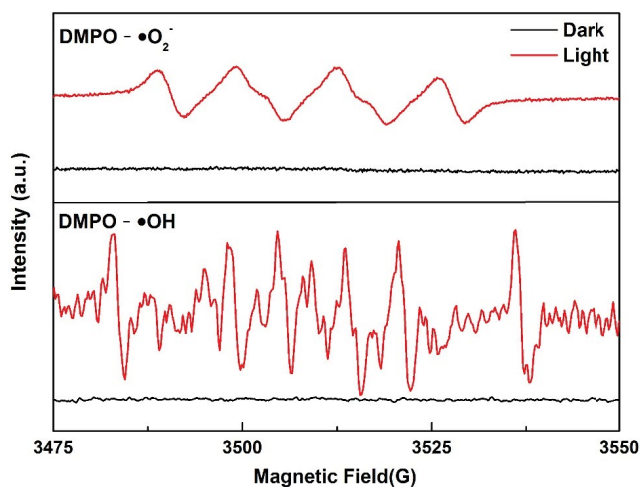


Fig. 8. ESR spectra of BiPO_4 nanosphere under dark and simulated solar light: $\text{DMPO}\cdot\text{O}_2^-$ in methanol dispersions and $\text{DMPO}\cdot\text{OH}$ in aqueous dispersions.

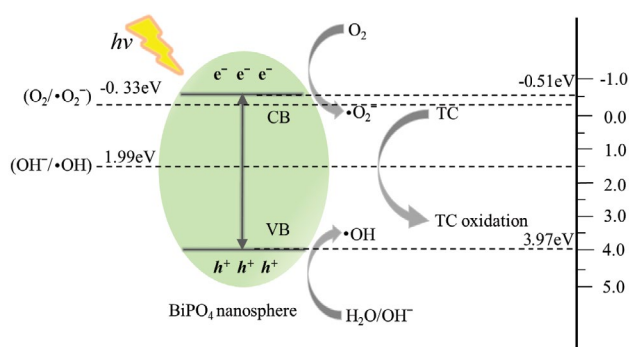


Fig. 9. Schematic diagram of photocatalytic degradation of TC with BiPO_4 nanospheres as photocatalyst under simulated solar light.

potential of BiPO_4 is more negative than the potential of superoxide radicals $\text{O}_2/\cdot\text{O}_2^-$ (-0.33 eV vs. NHE), and the VB potential of BiPO_4 is more negative than the potential of the hydroxyl radical $\cdot\text{OH}/\text{OH}^-$ (1.99 eV vs. NHE). As a result, the electrons in the conduction band of BiPO_4 can react with O_2 to form $\cdot\text{O}_2^-$ to degrade the pollutants [35]. The photo-generated holes in the VB of BiPO_4 can oxidize the hydroxyl ions to form hydroxyl radicals to degrade the pollutants [36]. Furthermore, the h^+ accumulated in the VB of BiPO_4 can directly degrade the organic substances.

4. Conclusion

The BiPO_4 nanospheres and the irregular BiPO_4 particles were successfully synthesized by a cost-effective hydrothermal method. The as-prepared samples showed excellent photocatalytic activity. The morphology, particle size and surface of the BiPO_4 nanospheres all influenced the degradation of TC. In addition, the photocatalytic ability of the BiPO_4 nanospheres was high when compared with the irregular BiPO_4 particles due to its special morphology. In short, BiPO_4 nanospheres are an economical semiconductor material and

a promising candidate with profound potential in the degradation of antibiotic wastewater.

Acknowledgments

This work is supported by the National Natural Science Foundation of China (21906039), Natural Science Foundation of Shaanxi Province (2019JQ-382), China Scholarship Council (No.201806560036), Funding project for introduced overseas scholars of Hebei Province (C20190321), Program for water resources research and promotion of Hebei Province (2019-55), Doctoral research fund of Hebei Geo University (BQ2019041).

References

- [1] Q. Bu, B. Wang, J. Huang, S. Deng, G. Yu, Pharmaceuticals and personal care products in the aquatic environment in China: a review, *J. Hazard. Mater.*, 262 (2013) 189–211.
- [2] F.R. Xiu, Y.F. Li, Y.Y. Qi, X. Yu, J.H. He, Y.W. Lu, X. Gao, Y.H. Deng, Z.Q. Song, A novel treatment of waste printed circuit boards by low-temperature near-critical aqueous ammonia: debromination and preparation of nitrogen-containing fine chemicals, *Waste Manage.*, 84 (2019) 355–363.
- [3] C.Y. Lu, W.S. Guan, T.K.A. Hoang, J.F. Guo, H.G. Gou, Y. Yao, Visible-light-driven catalytic degradation of ciprofloxacin on metal (Fe, Co, Ni) doped titanate nanotubes synthesized by a one-pot approach, *J. Mater. Sci. Mater. Electron.*, 27 (2016) 1966–1973.
- [4] F. Guo, M.Y. Li, H.J. Ren, X.L. Huang, W.X. Hou, C. Wang, W.L. Shi, C.Y. Lu, Fabrication of p-n $\text{CuBi}_2\text{O}_7/\text{MoS}_2$ heterojunction with nanosheets-on-microrods structure for enhanced photocatalytic activity towards tetracycline degradation, *Appl. Surf. Sci.*, 491 (2019) 88–94.
- [5] W.L. Shi, H.J. Ren, M.Y. Li, K.K. Shu, Y.S. Xu, C. Yan, Y.B. Tang, Tetracycline removal from aqueous solution by visible-light-driven photocatalytic degradation with low-cost red mud wastes, *Chem. Eng. J.*, 382 (2020) 122876–122883.
- [6] W.L. Shi, H.J. Ren, X.L. Huang, M.Y. Li, Y.B. Tang, F. Guo, Low-cost red mud modified graphitic carbon nitride for the removal of organic pollutants in wastewater by the synergistic effect of adsorption and photocatalysis, *Sep. Purif. Technol.*, 237 (2020) 116477–116484.
- [7] F. Guo, W.L. Shi, H.B. Wang, M.M. Han, W.S. Guan, H. Huang, Y. Liu, Z.H. Kang, Study on highly enhanced photocatalytic tetracycline degradation of type II $\text{AgI}/\text{CuBi}_2\text{O}_7$ and Z-scheme $\text{AgBr}/\text{CuBi}_2\text{O}_7$ heterojunction photocatalysts, *J. Hazard. Mater.*, 349 (2018) 111–118.
- [8] L. Bing, Z. Tong, Biodegradation and adsorption of antibiotics in the activated sludge process, *Environ. Sci. Technol.*, 44 (2010) 3468–3473.
- [9] D. Spasiano, R. Marotta, S. Malato, P. Fernandez-Ibanez, I.D. Somma, Solar photocatalysis: materials, reactors, some commercial, and pre-industrialized applications, a comprehensive approach, *Appl. Catal., B*, 170–171 (2015) 90–123.
- [10] F. Guo, M.Y. Li, H.J. Ren, X.L. Huang, K.K. Shu, W.L. Shi, C.Y. Lu, Facile bottom-up preparation of Cl-doped porous g- C_3N_4 nanosheets for enhanced photocatalytic degradation of tetracycline under visible light, *Sep. Purif. Technol.*, 228 (2019) 115770–115776.
- [11] W.L. Shi, F. Guo, S.L. Yuan, In-situ synthesis of Z-scheme $\text{Ag}_3\text{PO}_4/\text{CuBi}_2\text{O}_7$ photocatalysts and enhanced photocatalytic performance for the degradation of tetracycline under visible-light irradiation, *Appl. Catal., B*, 209 (2017) 720–728.
- [12] J. Xia, J. Di, H. Li, H. Xu, H. Li, S. Guo, Ionic liquid-induced strategy for carbon quantum dots/ BiOX ($X = \text{Br}, \text{Cl}$) hybrid nanosheets with superior visible-light-driven photocatalysis, *Appl. Catal., B*, 181 (2016) 260–269.
- [13] L.P. Wang, G.P. Yang, D. Wang, C.Y. Lu, W.S. Guan, Y.L. Li, J. Deng, J. Crittenden, Fabrication of the flower-flake-like

- CuBi₂O₄/Bi₂WO₆ heterostructure as efficient visible-light-driven photocatalysts: performance, kinetics and mechanism insight, *Appl. Surf. Sci.*, 495 (2019) 143521.
- [14] A. Fujishima, K. Honda, Electrochemical photolysis of water at a semiconductor electrode, *Nature*, 238 (1972) 37–38.
- [15] Q. Wu, R.V.D. Krol, Selective photoreduction of nitric oxide to nitrogen by nanostructured TiO₂ photocatalysts: role of oxygen vacancies and iron dopant, *J. Am. Chem. Soc.*, 134 (2012) 9369–9375.
- [16] M. Baradaran, F.E. Ghodsi, C. Bittencourt, E. Llobet, The role of Al concentration on improving the photocatalytic performance of nanostructured ZnO/ZnO:Al/ZnO multilayer thin films, *J. Alloys Compd.*, 788 (2019) 289–301.
- [17] J.F. Guo, P.T. Li, Z. Yang, A novel Z-scheme g-C₃N₄/LaCoO₃ heterojunction with enhanced photocatalytic activity in degradation of tetracycline hydrochloride, *Catal. Commun.*, 122 (2019) 63–67.
- [18] W.L. Shi, F. Guo, M.Y. Li, Y. Shi, M.J. Shi, C. Yan, Constructing 3D sub-micrometer CoO octahedrons packed with layered MoS₂ shell for boosting photocatalytic overall water splitting activity, *Appl. Surf. Sci.*, 473 (2019) 928–933.
- [19] L.P. Wang, T.T. Huang, G.P. Yang, C.Y. Lu, F.L. Dong, Y.L. Li, W.S. Guan, The precursor-guided hydrothermal synthesis of CuBi₂O₄/WO₃ heterostructure with enhanced photoactivity under simulated solar light irradiation and mechanism insight, *J. Hazard. Mater.*, 381 (2020) 120956–120967.
- [20] C.Y. Lu, F. Guo, Q.Z. Yan, Z.J. Zhang, D. Li, L.P. Wang, Y.H. Zhou, Hydrothermal synthesis of type II ZnIn₂S₄/BiPO₄ heterojunction photocatalyst with dandelion-like microflower structure for enhanced photocatalytic activity under simulated solar light degradation of tetracycline, *J. Alloys Compd.*, 811 (2019) 151976.
- [21] Y.F. Liu, Y.Y. Zhu, J. Xu, X.J. Bai, R.L. Zong, Y.F. Zhu, Degradation and mineralization mechanism of phenol by BiPO₄ photocatalysis assisted with H₂O₂, *Appl. Catal., B*, 142 (2013) 561–567.
- [22] C.S. Pan, Y.F. Zhu, New type of BiPO₄ oxy-acid salt photocatalyst with high photocatalytic activity on degradation of dye, *Environ. Sci. Technol.*, 44 (2010) 5570–5574.
- [23] M. Roming, C. Feldmann, Synthesis and characterization of nanoscaled BiPO₄ and BiPO₄:Tb, *J. Mater. Sci.*, 44 (2009) 1412–1415.
- [24] J.Y. Liu, Y. Bai, P.Y. Luo, P.Q. Wang, One-pot synthesis of graphene-BiOBr nanosheets composite for enhanced photocatalytic generation of reactive oxygen species, *Catal. Commun.*, 42 (2013) 58–61.
- [25] M. Gao, D. Zhang, X. Pu, H. Ma, C. Su, X. Gao, J. Dou, Surface decoration of BiOBr with BiPO₄ nanoparticles to build heterostructure photocatalysts with enhanced visible-light photocatalytic activity, *Sep. Purif. Technol.*, 170 (2016) 183–189.
- [26] Y.N. Zhang, H.Q. Fan, M.M. Li, Ag/BiPO₄ heterostructures: synthesis, characterization and their enhanced photocatalytic properties, *Dalton Trans.*, 42 (2013) 13172–13178.
- [27] J.Q. Li, H. Yuan, Z.F. Zhu, First-principles energy band calculation and one-step synthesis of N-doped BiPO₄, *J. Alloys Compd.*, 640 (2015) 290–297.
- [28] W. Maisang, A. Phuruangrat, C. Randorn, S. Kungwankunakorn, S. Thongtem, O. Wiranwetchayan, S. Wannapop, S. Choopun, S. Kaowphong, T. Thongtem, Enhanced photocatalytic performance of visible-light-driven BiOBr/BiPO₄ composites, *Mater. Sci. Semicond. Process.*, 75 (2018) 319–326.
- [29] H. Lv, Y. Liu, H. Tang, P. Zhang, J. Wang, Synergetic effect of MoS₂ and graphene as cocatalysts for enhanced photocatalytic activity of BiPO₄ nanoparticles, *Appl. Surf. Sci.*, 425 (2017) 100–106.
- [30] W.L. Shi, M.Y. Li, H.J. Ren, F. Guo, X.L. Huang, Y. Shi, Y.B. Tang, Construction of a 0D/1D composite based on Au nanoparticles/CuBi₂O₄ microrods for efficient visible-light-driven photocatalytic activity, *Beilstein J. Nanotechnol.*, 10 (2019) 1360–1367.
- [31] Y. Chen, X.L. Jin, P. Guo, Preparation of Fe₃O₄/BiPO₄ magnetic nanocomposite and its photocatalytic performance, *J. Mol. Struct.*, 1171 (2018) 140–149.
- [32] Q. Liang, J. Jin, C.H. Liu, S. Xu, C. Yao, Z.Y. Li, A stable BiPO₄/g-C₃N₄ nanosheet composite with highly enhanced visible-light photocatalytic activity, *J. Mater. Sci.- Mater. Electron.*, 29 (2018) 2509–2516.
- [33] Y. Guo, P.F. Wang, J. Qian, Y.H. Ao, C. Wang, J. Hou, Phosphate group grafted twinned BiPO₄ with significantly enhanced photocatalytic activity: synergistic effect of improved charge separation efficiency and redox ability, *Appl. Catal., B*, 234 (2018) 90–99.
- [34] G. Tan, L. She, T. Liu, C. Xu, H. Ren, A. Xia, Ultrasonic chemical synthesis of hybrid mpg-C₃N₄/BiPO₄ heterostructured photocatalysts with improved visible-light photocatalytic activity, *Appl. Catal., B*, 207 (2017) 120–133.
- [35] B.Y. Peng, S.S. Zhang, S.Y. Yang, H.J. Wang, H. Yu, S.Q. Zhang, F. Peng, Synthesis and characterization of g-C₃N₄/Cu₂O composite catalyst with enhanced photocatalytic activity under visible light irradiation, *Mater. Res. Bull.*, 56 (2014) 19–24.
- [36] F. Dong, Z.Y. Wang, Y.H. Li, W.K. Ho, S.C. Lee, Immobilization of polymeric g-C₃N₄ on structured ceramic foam for efficient visible-light photocatalytic air purification with real indoor illumination, *Environ. Sci. Technol.*, 48 (2014) 10345–10353.